PHYSICAL REVIEW B VOLUME 35, NUMBER 6 15 FEBRUARY 1987-II

Influence of the supercell structure on the folded acoustical Raman line intensities in superlattices

B. Jusserand and D. Paquet
Centre National d'Etudes des Télécommunications, Laboratoire de Bagneux, 196 Avenue Henri Ravera, 92220 Bagneux, France

F. Mollot
Laboratoire de Microelectronique et Microstructures, Centre National de la Recherche Scientifique, 196 Avenue Henri Ravera, 92220 Bagneux, France

F. Alexandre and G. Le Roux
Centre National d'Etudes des Télécommunications, Laboratoire de Bagneux, 196 Avenue Henri Ravera, 92220 Bagneux, France
(Received 12 August 1986)

We compare forward and backward Raman scattering results on folded acoustical phonons in GaAs-AlAs superlattices with a detailed theoretical analysis of their dispersion properties and light scattering activity. By forward scattering, which involves phonons with a vanishing wave vector, we first get evidence of zone-center gaps, in quantitative agreement with the elastic model predictions. We also check the zone-center selection rules and conclusively prove the assignment of the light scattering on folded acoustical phonons to a modulated photoelastic (Brillouin) process. In backscattering experiments, one creates phonons with a finite wave-vector and the zone-center selection rules are relaxed. We quantitatively describe this phenomenon, and demonstrate that the backscattering intensities directly reflect the coupling between folded branches and the related zone-boundary gap magnitude. An excellent agreement between measured and calculated intensities is obtained. Finally we emphasize the great sensitivity of the gaps and intensities, contrary to the backscattering frequency shifts, to the supercell inner structure. This greatly enhances the interest of Raman scattering as a tool for characterizing periodic structures.

I. INTRODUCTION

The salient effects of the new periodicity and of the corresponding Brillouin zone folding on the acoustical phonons in superlattices are well understood.[1] The acoustical vibrations propagate in both layer compounds and the dispersion curves are obtained (i) by folding the acoustical dispersion curve of an average compound and (ii) by opening small gaps at zone center and zone edge. These features have been described quantitatively in the frame of the elastic model.[2] Raman backscattering (BS) has been used extensively to study these folded modes.[3–11] As emphasized in Ref. 5, a striking feature appears in the analysis of the BS results in superlattices: the wave vector of the phonon created by BS is not negligible and can even be of the same order of magnitude as the Brillouin zone extension. As a consequence, the experimental results, though clearly demonstrating the folding of the Brillouin zone, are actually unsensitive to the gap openings. Another striking feature of the BS spectra is the selection rules: the BS lines are always observed in the parallel configuration and never in the perpendicular one. This is in contradiction with the standard Raman selection rules which predict that some lines must appear in parallel and the other ones in perpendicular configuration. On the other hand, a Brillouin scattering mechanism can also be invoked for these lines of acoustical origin.[12] The corresponding selection rules then predict that zone-center phonons are either forbidden or only observable in parallel configuration.

In this paper we shall first revisit the theory of folded acoustical phonons in superlattices, focusing on zone-center gaps and on the photoelastic intensity of the Raman lines. Experimental results on forward scattering (FS) already published in Ref. 13 will be analyzed in more detail. We thereby get evidence of zone-center gaps whose magnitude varies with the supercell structure as predicted by the theory. Furthermore, we present a detailed analysis of the line intensities out of the Brillouin zone center. Our results, which are quantitatively different from those obtained from the Green function calculation of Ref. 14, show that the dominant contribution comes from the modulation of the photoelastic response[6] in the supercell (which was not taken into account in Ref. 14). We quantitatively account for the softening of the zone-center selection rules and then demonstrate the effects of the zone-center gaps on the BS spectra.

The paper is organized as follows. Sections II and III are devoted to the theoretical considerations. In Sec. II A we shall focus on the acoustical gaps in the frame of the elastic model, in Sec. II B we shall present the Fourier transform analysis of the wave equation, and in Sec. III we shall calculate the photoelastic activity of the folded modes. Sections IV–VI are devoted to experiments on GaAs-AlAs superlattices and discussion. In Sec. IV we shall present and analyze the forward scattering results and compare the measured gaps with the theoretical predictions, in Sec. V a large number of BS results are

presented and the intensity of the lines are analyzed according to the considerations of Sec. III, Sec. VI will be finally devoted to some samples with more complex supercell structures.

II. DETAILED ANALYSIS OF THE FOLDED ACOUSTICAL DISPERSION CURVES

The equation of motion for propagation along the growth axis z of longitudinal elastic waves in a superlattice is

$$\frac{\partial}{\partial t}\left[\rho(z)\frac{\partial u}{\partial t}\right]-\frac{\partial}{\partial z}\left[C(z)\frac{\partial u}{\partial z}\right]=0\ , \tag{1}$$

where u, ρ, and C are, respectively, the longitudinal displacement, the local density, and the elastic constant C_{11}. In what follows we shall only deal with periodic structures of period d. The natural method to solve (1) is to use Fourier transform, as will be discussed at length in Sec. II B. The principal advantages of this method are that it can be used for any periodic variation of ρ and C, for instance, in a superlattice with broaden interfaces,[15] and that we find it easier to understand the scattering efficiency of each mode. On the other hand, in the usual case where the superlattice is made of a stacking of two layers of different materials with abrupt interfaces, one has at one's disposal the exact well-known solution given by Rytov,[2] which is the elastic version of the electronic Kronig-Penney model. This model has been extensively used in the literature to analyze Raman experiments in superlattices and provides an excellent description of the experimental results. In the following paragraph we shall focus on its predictions about the gaps amplitude.

A. Gaps and dispersion from Rytov's model

The exact dispersion relation of folded acoustical modes from the elastic model read as

$$\cos(Qd)=\cos\left[\omega\left[\frac{d_A}{v_A}+\frac{d_B}{v_B}\right]\right]-\frac{\epsilon^2}{2}\sin\left[\omega\frac{d_A}{v_A}\right]\sin\left[\omega\frac{d_B}{v_B}\right]\ , \tag{2}$$

where d_A,d_B are the thickness of the two constituting layers, v_A,v_B the sound velocities in the corresponding bulk compounds, and Q the superlattice wave vector and where the coefficient

$$\epsilon=(C_B\rho_B-C_A\rho_A)/(C_B\rho_B+C_A\rho_A)$$

is a measure of the mismatch of the two acoustical impedances. ϵ is usually small and, for the case we study all along the paper, i.e., GaAs-AlAs superlattices, it amounts to 0.18, as deduced from handbook values of the whole parameters of the model, except for the AlAs acoustical velocity whose value (5.7×10^5 cm/s) has been fitted on a large number of folded lines frequencies. Thus at zeroth order, the dispersion relation reduces to

$$\cos(Qd)=\cos\left[\omega\left[\frac{d_A}{v_A}+\frac{d_B}{v_B}\right]\right]\ ,$$

i.e., to the exact folding of the one of a bulk compound with a sound velocity defined through

$$\frac{d}{v}=\frac{d_A}{v_A}+\frac{d_B}{v_B}\ . \tag{3}$$

This relation simply means that the transit time through a period is the sum of the transit times through each layer. We thus find doubly degenerate zone-center (ν even) or zone-edge (ν odd) modes at frequencies

$$\Omega_\nu=\nu\frac{\pi v}{d}\ .$$

A straightforward expansion of (2) in first order in ϵ^2 leads to a gap opening $\mathcal{G}_\nu$, symmetric around Ω_ν, which amounts to

$$\mathcal{G}_\nu=\frac{2v}{d}\left|\epsilon\sin\left[\pi\nu\frac{(1-x)v_B}{(1-x)v_B+xv_A}\right]\right|\ .$$

Here x is the average concentration of compound B, i.e., $x=d_B/d$. We have plotted on Fig. 1 the ratio $\mathcal{G}_\nu/\Omega_\nu$ as a function of x, for $\nu=1$ to 4. Note that this ratio does not depend on the period d and that every zone-center gap vanishes at a critical concentration value:

$$x_c=\frac{v_B}{v_A+v_B}\quad\text{(is 0.55 for GaAs-AlAs)}\ . \tag{4}$$

When the wave vector Q increases from zero, the separation between the two branches originating from $\Omega_{2\nu}+\mathcal{G}_{2\nu}/2$ increases, due to the dispersion. For small values of Q, the splitting $\mathcal{G}_{2\nu}(Q)$ of such a doublet is

$$\mathcal{G}_{2\nu}(Q)=[\mathcal{G}_{2\nu}(0)^2+4v^2Q^2]^{1/2}$$

The two contributions are of the same order of magnitude

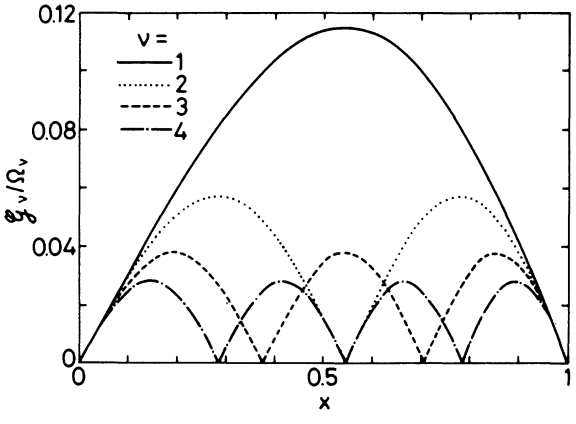

FIG. 1. Zone-center ($\nu=2,4$) and zone-edge ($\nu=1,3$) acoustical gaps $\mathcal{G}_\nu$ normalized to the corresponding average frequency Ω_ν as a function of the Al average concentration x in GaAs-AlAs superlattices. This quantity does not depend on the period of the structure.

for $Qd=\epsilon$. In the case of GaAs-AlAs superlattices ($\epsilon\sim 0.18$) and in a Raman backscattering experiment where the typical value of Q is 10^6 cm^{-1}, this leads to $d=18$ Å, a rather small period. As a consequence, for larger-period superlattices, the doublet splitting observed in backscattering will reflect essentially the dispersion. Such an experiment is thus unable to test the zone-center gap amplitudes. However, as will be discussed in Sec. IV, Raman forward scattering experiments create phonons with a wave vector fulfilling the relation $Qd \ll \epsilon$. Such an experiment thus allows a study of the zone-center gaps. An indirect but experimentally easier way to study these zone-center gaps is to analyze, in a backscattering experiment, the relative intensities of the folded lines. To present such an analysis, we consider more suitable to treat the lattice dynamics, solving Eq. (1) by Fourier transform. It is the purpose of the next section.

B. Gaps and dispersion from a Fourier analysis

As the medium is periodic, the mass density $\rho(z)$ and the elastic constant $C(z)$ can be expanded in Fourier series:

$$\rho(z)=\sum_n \rho_n e^{inGz},$$

$$C(z)=\sum_n C_n e^{inGz},$$

where $G=2\pi/d$. Applying Bloch theorem, the displacement field can also be written as

$$u_Q(z)=e^{iQz}\sum_n u_{n,Q}e^{inGz},$$

where Q is the superlattice wave vector. Substituting in Eq. (1) and assuming harmonic time behavior, one obtains the set of following equations:

$$\sum_n \{[\omega^2(Q)\rho_{m-n}-C_{m-n}(Q+nG)(Q+mG)]u_{n,Q}\}=0 . \tag{5}$$

The task is now to solve the secular equation of this infinite system. In a nonpathological system, the modulus of the Fourier components ρ_i and C_i are rapidly decreasing functions of i, a fact which justifies the truncation of the infinite matrix appearing in (5). The most drastic approximation consists in retaining only ρ_0 and C_0. This leads to the dispersion relation

$$\omega^2_{p,Q}=\frac{C_0}{\rho_0}(Q+pG)^2$$

which corresponds to the folding of an average bulk acoustic dispersion curve with sound velocity $v_0=(C_0/\rho_0)^{1/2}$. Note that this average velocity differs from the one obtained from Rytov's model [Eq. (3)]. To get a gap opening at zone center, one needs to couple $u_{n,Q=0}$ with $u_{-n,Q=0}$, i.e., to use degenerate perturbation theory, as already done in Ref. 6. This coupling involves ρ_{2n} and C_{2n} which are rather small for large n. At zone boundary, one needs to couple $u_{n,Q=G/2}$ with $u_{-n-1,Q=G/2}$ to lift the degeneracy. A more detailed analysis in the abrupt interface case shows that to obtain numerical results close to the exact ones, we need to deal with coupling through $\rho_{1,2}$ and $C_{1,2}$ which are the largest off-diagonal nondegenerate perturbations. When accounting for these nonresonating corrections, the vanishing of the first zone-center gap shifts from a concentration $x=0.5$ to $x=x_c$ as given by (5).

We have plotted on Fig. 2 the Fourier components $0,\pm1,\pm2$ of two lower-energy folded branches, calculated as a function of Q ranging on the whole Brillouin zone, for a GaAs-AlAs structure with abrupt interfaces and $x=0.3$. Taking advantage of the existence of symmetry planes located in the middle of each layer, we chose the coordinates origin on one of these planes to obtain real Fourier components. As can be seen from the figure, for a Q value far from zone center and zone edge, each eigendisplacement mode can be correctly described by its major Fourier component $u^{(p)}_{p,Q}$ [$(u^{(p)}_{p,Q})^2/\sum_n (u^{(p)}_{n,Q})^2 \sim 0.99$], a fact which provides a natural labeling of the folded branches. On the contrary, as Q reaches zone center or zone boundary, the two degenerate Fourier components take equal absolute values. The $p\pm1$ components, although smaller, remain significant on the whole Brillouin zone. As the composition profile is symmetric relative to each midlayer plane, the eigendisplacements at zone center are either symmetric ($u_{n,Q=0}=u_{-n,Q=0}$) or antisymmetric ($u_{n,Q=0}=-u_{-n,Q=0}$). Each doublet then consists of a symmetric and an antisymmetric mode, which can be labeled by the corresponding representation B_2 (symmetric) or A_1 (antisym-

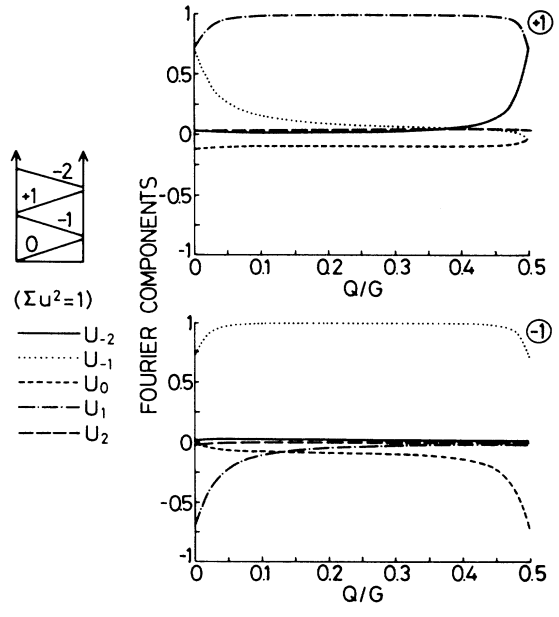

FIG. 2. Major Fourier components $u^{(p)}_{n,Q}$ ($n=0,\pm1,\pm2$) of the two lowest folded modes ($p=\pm1$) as a function of the wave vector Q normalized to the unit reciprocal-lattice parameter G for a GaAs-AlAs abrupt structure with $x=0.3$.

metric) of the superlattice tetragonal point group. In the following section we shall apply this Fourier analysis to describe the Raman efficiency.

III. SCATTERING EFFICIENCY OF FOLDED ACOUSTICAL MODES

Assuming, as justified by experiment, that the light scattering on folded acoustical phonons originates from the photoelastic effect, the local transverse Stokes polarization can be written as

$$P(z)=\Pi(z)\frac{\partial}{\partial z}[u(z,t)]E_i(z,t) ,$$

where $\Pi(z)$ is the local value of the photoelastic tensor element Π_{12} (we assume the medium to be locally cubic) and $E_i(z,t)$ is the transverse electric field produced by the incident beam. Following Colvard *et al.*,[6] we shall derive the scattering intensity by expanding $\Pi(z)$ also in Fourier series, our aim being to obtain numerical predictions to be compared with experimental results. The Stokes polarization due to a mode with superlattice vector $-Q$ in branch p and an electric field with wave vector q_i displays spatial variation $P(z)=P_{q_i-Q}(z)e^{i(q_i-Q)z}$, where $P_{q_i-Q}(z)$ is a periodic function. The scattering efficiency only depends on its constant part, i.e., the polarization by unit length, which is

$$P_{0,q_i-Q}=\sum_h \left[\Pi_{-n}u^{(p)}_{n,-Q}(nG-Q)\right]E_i .$$

Normalizing the displacement field to unity, i.e., $\sum_n u_{n,Q}u_{-n,Q}=1$, and thus using the corresponding thermal factor, the scattering intensity per unit length takes the form

$$I_p(\omega_i-\omega_{p,-Q})\propto \frac{n(\omega_{p,-Q})+1}{\omega_{p,-Q}} \times E_i^2\left[\sum_n \Pi_{-n}u^{(p)}_{n,-Q}(nG-Q)\right]^2 . \tag{6}$$

From this expression we can calculate the line intensities for any given periodic structure and any sample temperature, provided we know the photoelastic coefficient profile. The room-temperature intensity of the lines only depends, within a good approximation, on the concentration x and the product Qd and not explicitly on the energy of the mode. The thermal factor can be indeed reduced at high temperature ($kT \gg h\omega$) to T/ω and I:

$$I_p(\omega_i-\omega_{p,-Q})\propto \frac{T}{v^2}\left[\sum_n \Pi_{-n}u^{(p)}_{n,-Q}\frac{2\pi n-Qd}{2\pi p-Qd}\right]^2 E_i^2 ,$$

where we used the approximate relation

$$\omega^2_{p-,Q}=v^2(pG-Q)^2 .$$

Before considering in more details the case of the GaAs-AlAs abrupt structure, we already can determine the zone-center selection rules for symmetric profiles. As explained in Sec. II B, for such profiles, zone-center doublets consist of symmetry and antisymmetric modes. The zone-center scattering intensity

$$I_p(\omega_i-\omega_{p-,Q})\propto \frac{n(\omega_{p,0})+1}{\omega_{p,0}}E_i^2G^2\left[\sum_n n\Pi_{-n}u^{(p)}_{n,0}\right]^2$$

then vanishes for the symmetric mode and we recover the Brillouin scattering selection rules.

To analyze the softening of these selection rules for nonvanishing Q values, we show in Fig. 3 the room-temperature intensity of the lines $\pm1,\pm2$ for an abrupt GaAs-AlAs structure, as a function of the composition x and the wave vector Q. We took $\Pi_A=1$ (GaAs) and $\Pi_B=0.1$ (AlAs) as justified by the experimental results (see Sec. V). At zero wave vector, one recovers the Brillouin selection rules: for $x<x_c$ the scattering on the -1 mode is allowed (antisymmetric displacement, symmetric strain), the scattering on the $+1$ mode being forbidden. At $x=x_c$ the gap vanishes which corresponds to the crossing of the symmetric and antisymmetric modes. At $x>x_c$ the allowed mode becomes the high-energy one in the doublet (i.e., the $+1$ mode). Similar features appear for the ±2 modes with three vanishings of the gap and three crossings of the symmetric and antisymmetric modes.

For a Q vector ranging around $0.25G$, the Fourier component $u^{(p)}_{p,Q}$ becomes the most important one for mode p (see Fig. 2). As a consequence, the dependence of the scattering intensity as a function of x merely reflects the dependence on x of the Fourier component Π_{-p} of the photoelastic profile. In other words, as Q increases from zone center, the symmetric and antisymmetric components of the displacement field mix together, and the asymmetry of the scattering intensity within a doublet rapidly decreases from 1 to a small value. Finally, near zone edge, the component $u^{(p)}_{p,Q}$ of branch p decreases as $u^{(p)}_{-p-1,Q}$ increases, and the scattering intensity as a function of x displays oscillations which reflect the oscillations of the zone-edge gap.

Raman backscattering experiments in superlattices test phonons whose wave vector typically ranges from $0.06G$ to $0.3G$ (depending on the period). Thus experiment with small period samples will allow, through the analysis of the relative line intensities, to obtain evidence of the coupling near zone center between the $u^{(p)}_{p,Q}$ and $u^{(p)}_{-p,Q}$ components. The variation of this relative intensity as a function of x directly reflects the gap variation. Such a backwards experiment, quite easier to perform than a forward one, will thus provide good information on the zone-center properties. Furthermore the scattering intensity [Eq. (6)] can be spit into two terms:

$$I_p(\omega_i-\omega_{p,-Q})\propto \frac{n(\omega_{p,-Q})+1}{\omega_{p,-Q}} \times E_i^2\left[-Q\Pi_0u^{(p)}_{0,-Q} + \sum_{n\,(\neq0)}\Pi_{-n}u^{(p)}_{n,-Q}(nG+Q)\right]^2 .$$

The first one ($n=0$) is proportional to Π_0, the average of

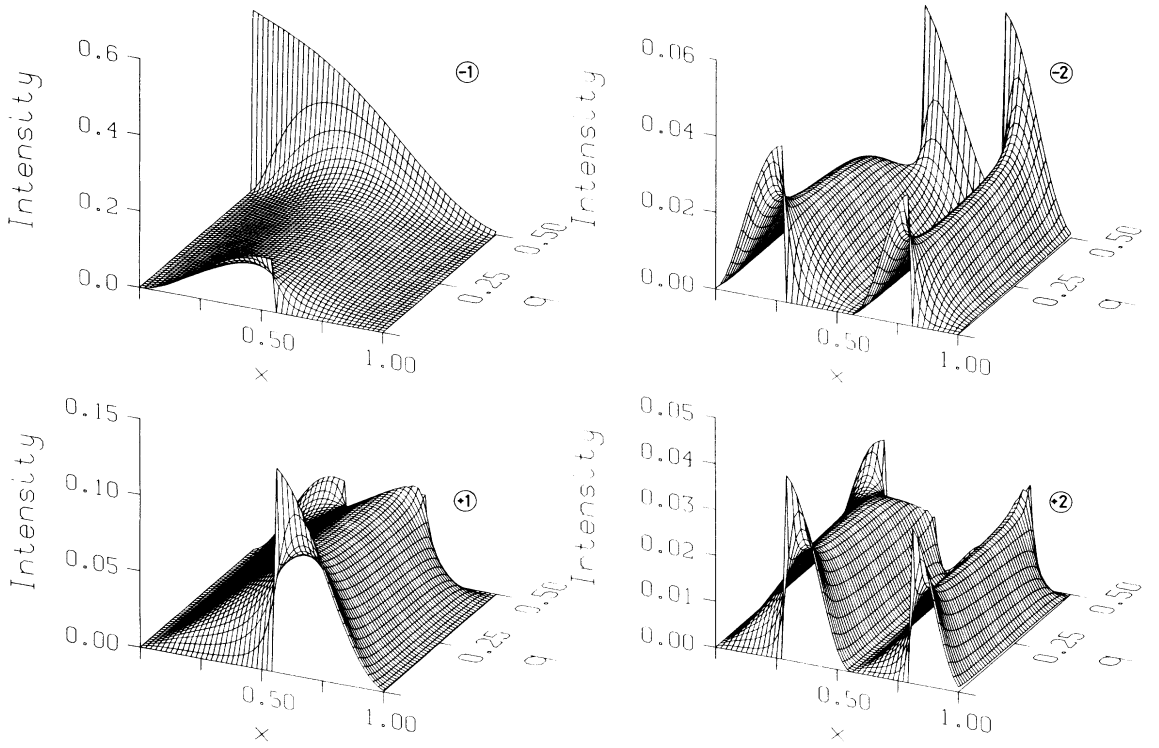

FIG. 3. Room-temperature intensity of the $\pm 1, \pm 2$ folded lines as a function of the Al concentration x and the wave vector q normalized to the unit reciprocal-lattice parameter G calculated for a GaAs/AlAs abrupt structure. The intensity units are arbitrary but the same for the four lines.

the photoelastic coefficient on a period and the second one ($n \neq 0$) is proportional to the difference of the photoelastic constants of both compounds. The presence of a term in Π_0 in the intensity of the folded lines is due to the existence of the nonresonant couplings introduced in Sec. II B. As shown later, this term, though not changing the trends of the effects and though induced by small Fourier components of the displacement, is essential to reproduce quantitatively the BS intensities. A quantitative analysis of the measured line intensities will thus provide an estimate of the ratio of the two bulk photoelastic constants.

IV. FORWARD SCATTERING RESULTS AND THE ZONE CENTER GAPS

To probe the zone-center frequencies and selection rules in superlattices, we must perform forward scattering (FS) experiments. In this configuration the wave vector of the created phonon is much smaller than in the usual BS configuration. We show in Fig. 4 the different experimental configurations used in this work. Due to the high value of the refractive index of the samples ($n \sim 4.0$), the propagation inside the structure is near perpendicular to the surfaces whatever the light incident angle. The created phonon wave vector is thus approximated by

$$Q = k_i + k_s \quad \text{(BS)},$$

$$Q = k_i - k_s \quad \text{(FS)},$$

where $k_{i,s} = 2\pi n / \lambda_{i,s}$ are the wave vectors inside the sample of the incident (i) and scattered (s) light. These quantities are nearly equal and one obtains

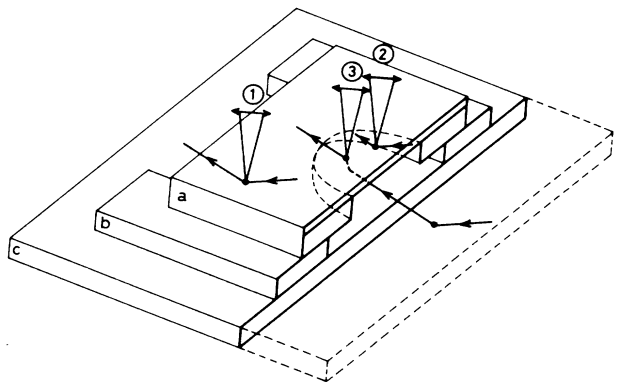

FIG. 4. Sketch of the sample mounting and of the light scattering configurations used in the forward scattering (FS) experiment. The front half part has been removed for clarity. The sample (a) is mounted on a metallic mirror (c) through wedges (b) so that one passes from the backscattering configurations (1 and 2) to the FS one (3) by only a translation. For each configuration we show the incident and reflected beams as well as the angle of signal collection. As FS is concerned, the incident light reaches the superlattice backface after a reflexion on the mirror.

$Q \sim 4\pi n/\lambda_i$ (BS),

$Q \sim 0$ (FS).

For usual laser lines ($\lambda_i \sim 5000$ Å) Q_{BS} is of the order of 10^6 cm^{-1}, a value which prevents, as explained in Sec. II A, the observation of the zone-center gaps in our structures whose period is larger than 30 Å. On the contrary, the FS experiment always probes zone center. The latter method however is very difficult to use in GaAs-AlAs structures. The samples are indeed opaque to the Ar^+- and Kr^+-ion laser lines, essentially because of the thick GaAs substrate. We therefore removed the substrate on a small area, using a selective chemical etching procedure. On this window, we can obtain FS spectra provided the superlattice layer is sufficiently transparent. We succeeded in performing the experiment on two samples:

$S1$: $d = 45$ Å $x = 0.48$,

$S2$: $d = 36$ Å $x = 0.72$.

These parameters, and those of all the samples used in this work, have been determined by simple and double x-ray diffraction. We chose short period samples in order to maximize the zone-center gaps which scale on d^{-1} and also to increase the optical absorption edge energy. In both samples we obtained the best spectra using an incident energy just below the superlattice absorption edge, taking advantage of the indirect character of these samples.[16] The luminescence signal which usually prevents the observation of Raman signals in these conditions is thereby much reduced in intensity and shifted to lower energies.

We present in Fig. 5 the spectra in the frequency range of the first doublet obtained in parallel configuration on both samples for the three different configurations shown in Fig. 4: BS out the window area (1), BS on the window area (2), and FS (3). The latter one is dominated by a single line located between the two components of BS doublet. As no line is observed in perpendicular configuration, the Brillouin selection rules are fulfilled and the FS line is attributed to the single allowed zone-center mode (A_1 representation). As the other line within the zone-center doublet is forbidden, we cannot directly obtain from the FS spectra alone any estimate of the zone-center gap. We can however extract this quantity from the comparison between FS and BS spectra, assuming the theoretical result that the average frequency between modes $+1$ and -1 is independent of Q. From the shift between the FS line and the average frequency of the BS doublet, we determine the zone-center gap $\mathcal{G}_2 = \omega_{B2} - \omega_{A2}$ which compares very well with the theoretical predictions, as shown in Fig. 6. In this figure the theoretical curve is the same as in Fig. 1, but with a negative value for $x > x_c$ to account for the different symmetry of the modes.

In the spectra obtained on the window, we see also some smaller contributions due to BS in the FS results and FS in the BS ones. These contributions appear as small lines on $S1$ and shoulders on $S2$. We assign them to internal reflections on the surface of superlattice layer. A similar reflection is negligible in the usual BS spectra because of the small refractive index mismatch between the superlattice and the substrate.

We thus obtain the first experimental determination of the lower-zone-center acoustical gap whose magnitude agree very well with the elastic model predictions. This result is a more accurate test of the model than the usual backscattering frequency measurements. These latter quantities are indeed essentially sensitive to the period value and not to the detail of the supercell structure. On the contrary, the gap is essentially sensitive to the super-

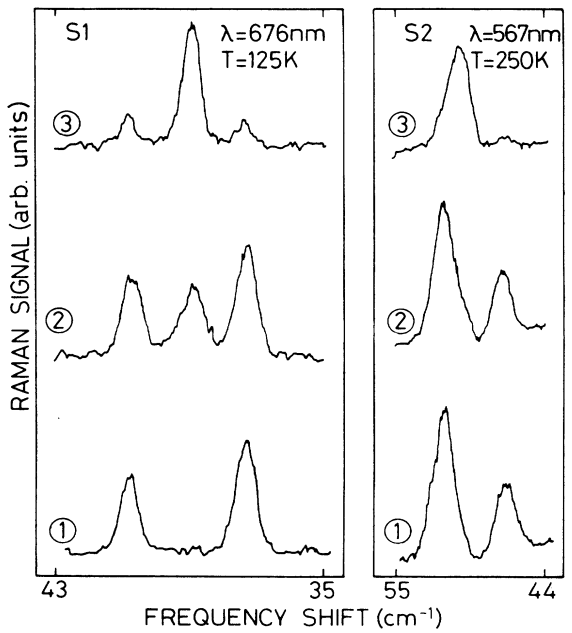

FIG. 5. Raman spectra of samples $S1$ and $S2$ (see text) for the three different configurations shown in Fig. 4 with the same labeling.

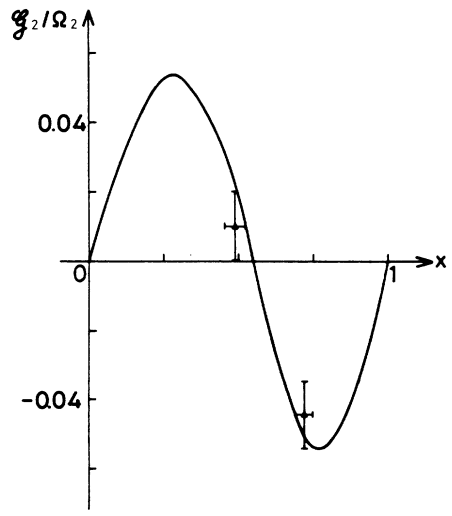

FIG. 6. Normalized first zone-center gap as a function of the concentration x. The experimental results (triangles) are compared with the calculation (solid line).

lattice modulation characteristics. The practical limitations in the FS measurements however make difficult a systematic study of the gap variations using this method. We will thus, in what follows, focus on the coupling between folded modes and analyze the BS intensities which are directly related to the zone-boundary gaps. One can get a first feeling of this relation in the previous results. On both samples, the allowed zone-center mode is shifted from the BS doublet average frequency towards the higher intensity BS component. On $S1$ ($x=0.48$) this shift is very small and the BS intensity "asymmetry" $(I_{-1}-I_{+1})/(I_{-1}+I_{+1})$ is also very small. On the contrary, for $S2$ ($x=0.72$) both the shift and the asymmetry are large.

V. BACKSCATTERING LINE INTENSITIES

We analyzed in Sec. III the variation as a function of x and Qd of the successive folded lines. These lines are observed on all the sample and usually two or three doublets are detected. We present in Fig. 7 two typical Raman spectra obtained at room temperature in this frequency range and in nonresonant conditions. As already shown in Ref. 6 large variations of the folded lines intensities appear near resonance with electronic transitions and the photoelastic description is no longer valid. The relative intensities of the various lines shown in Fig. 7 clearly display rich and complex variations. Each doublet can display a negative or positive asymmetry, the ratio between the average intensity of doublet 2 and doublet 1 fluctuating with a value smaller than 1. To analyze these two spectra, we use the curves shown in Fig. 7 which display the two corresponding values of Qd for the variation of the intensity of the four lower folded lines as a function of x. These diagrams are sections of the surfaces shown on Fig. 3 at $Q/G=0.06$ and 0.17, respectively. The vertical line on each diagram corresponds to the actual composition x of the related sample. The agreement between experiment and theory is good as concerns the average intensity and the asymmetry. These diagrams shapes are dominated by the following two parameters.

(i) The value of the corresponding dominant Fourier component Π_{+p} of the photoelastic coefficient which drives the oscillating variation of the average doublet intensity as a function of x and which is independent of Qd.

(ii) The value of the corresponding zone-center gap which drives the doublet asymmetry oscillating variation. This contribution decreases with increasing Qd. It induces the crossing of the intensities of lines $+p$ and $-p$ around each gap vanishing concentration.

Up to now, we only referred to the dominant Fourier components and the resonant couplings. The effect of the nonresonant couplings and namely of the coupling with the 0 component of the $+1$ modes is small for small values of Qd (sample $S3$). For intermediate values of Qd, the coupling with the $n=0$ Fourier component through Π_0 becomes however significant. As it appears with a different coefficient in the intensities I_{+1} and I_{-1}, it gives an extra contribution to the doublet asymmetry. This effect can be felt on the diagrams of Fig. 7 through the intensity decrease of line $+1$ relative to line -1 from $S3$ to $S4$. As already outlined in Eq. (6), the presence of this Π_0

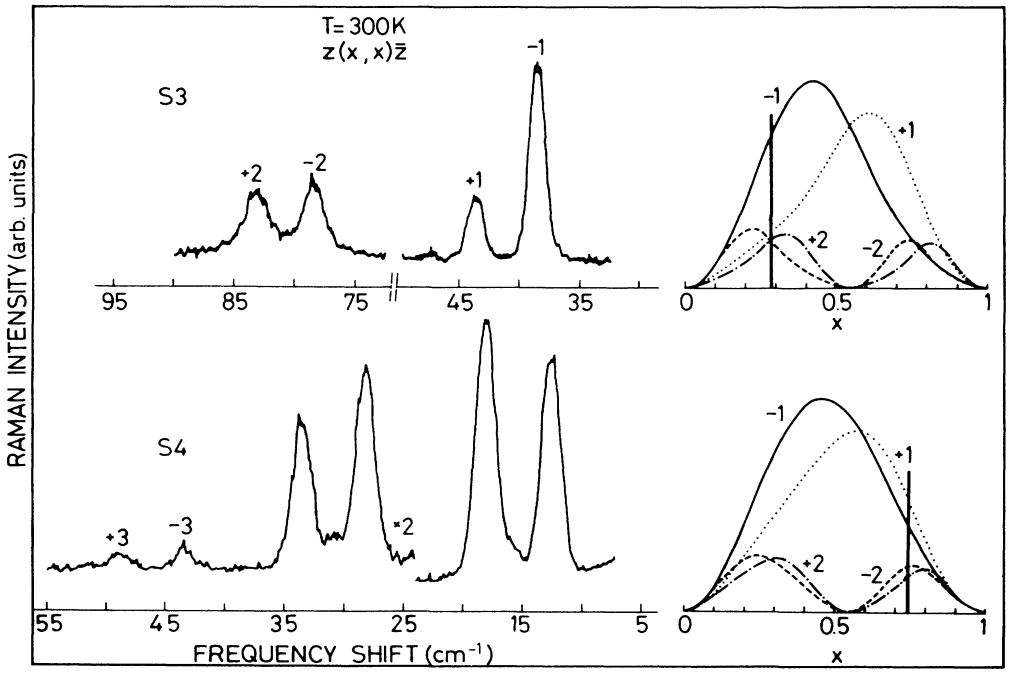

FIG. 7. Raman spectra of samples $S3$ ($d=40$ Å, $x=0.29$) and $S4$ ($d=115$ Å, $x=0.74$) compared with the corresponding sections of the surfaces shown on Fig. 3.

contribution will allow an estimate of the relative value Π_B/Π_A of the two bulk photoelastic coefficients.

We studied the asymmetry of the first doublet on two series of samples with various x but fixed period ($d \sim 40$ and 100 Å). On each sample we measured the asymmetry for various laser lines looking for an energy range for which the asymmetry remains constant, thus getting rid of any electronic resonance effect. The measured asymmetries are shown in Figs. 8(a) and 8(b) as a function of x and compared with the theory. The calculated variation with x of the asymmetry is shown on each figure for various values of Π_B/Π_A. The first clear result is the very good agreement in the amplitude of the oscillation. This quantity depends only slightly on the unknown ratio (provided it is not too close from 1) and the agreement thus obtained without any fit. The amplitude of the oscillation decreases with increasing Qd (0.85 for the 40-Å series; 0.35 for the 100-Å one), which clearly illustrate the progressive softening of the zone-center selection rules. Furthermore, for a given value of Qd, the average over x of the intensity asymmetry varies as a function of Π_B/Π_A and the variation is more pronounced for larger values of Qd. From the whole experimental values, we demonstrate that Π_{AlAs} is lower than Π_{GaAs}. From the values on the 100 Å series, we can roughly estimate that $\Pi_{AlAs}/\Pi_{GaAs} \sim 0.1$. We thus find a much smaller photoelastic coefficient for AlAs than for GaAs, a result in good agreement with the theoretical result[17] quoted in Ref. 6 and with an extrapolation of experimental values in GaAlAs.[18] One must emphasize that the photoelastic modulation in GaAs-AlAs superlattices is very large which induces intense folded lines and favors their observation. This feature also limits the influence of the $n=0$ terms on the asymmetry of the first folded doublet and thus the precision of the above estimation. But even in this case, a detailed analysis as presented here is needed to reproduce quantitatively the experimental results. In the calculation of Babiker *et al.*,[14] the local photoelastic coefficient is assumed constant along the superlattice axis and the predicted folded intensities are extremely small, in contrast with the experimental results on GaAs-AlAs structures. In their treatment, these intensities originate only from the $n=0$ component of the folded modes, which remains very small unless the two bulk constituents have very different acoustical properties. On the other hand, the linewidths are dominated in our experiment by the instrumental response function. We thus did not consider any line-broadening effects in our calculation. Furthermore, the line shape predicted in Ref. 14 comes from interference effects between the wings of the strong $n=0$ line and the weak folded ones. In our case, where the folded modes scattering activity is much larger, these effects are negligible.

Another application of our model can be found in the analysis of periodic structures with more complex supercells, where an exact solution is not currently available. Moreover, as already outlined before, the folded BS intensities, contrary to their frequencies are sensitive to the detail of the structure. An analysis of them is thus needed to characterize the shape of the periodic variation, as shortly illustrated in the following section.

VI. INFLUENCE OF THE SUPERCELL STRUCTURE

We present in Fig. 9 a Raman BS spectra obtained in nonresonant conditions, in parallel configuration on a sample whose supercell is made of four different layers: 30 Å of GaAs, 85 Å of AlAs, 30 Å of GaAs, and 190 Å of AlAs. In this sample, the BS wave vector amounts to around $0.5G$, i.e., we probe the zone-edge vibrations. The lines labeled 1–6 are thus assigned to unresolved zone-edge doublets, which are equidistant. Line n corresponds

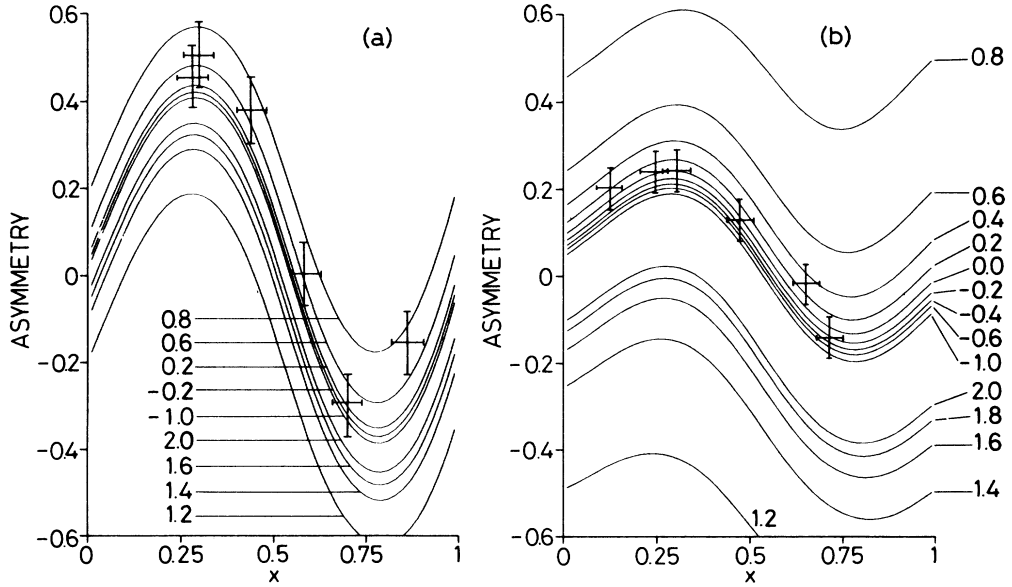

FIG. 8. Measured first Raman doublet asymmetry as a function of the average Al concentration x in GaAs-AlAs abrupt structures, compared with the calculation for various values of Π_B/Π_A. (a) $d=40$ Å; (b) $d=100$ Å.

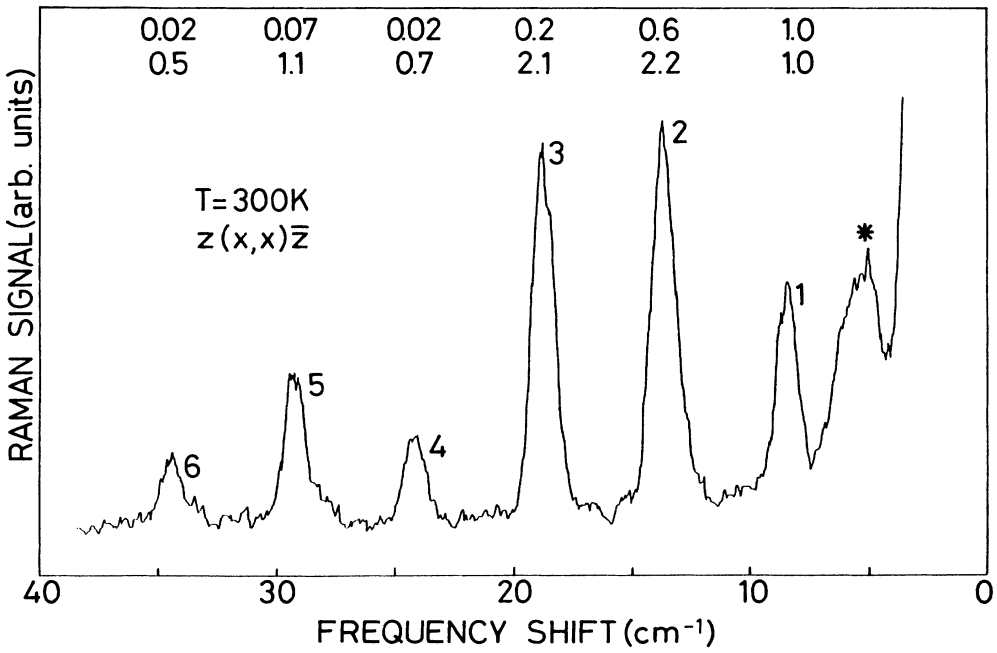

FIG. 9. Raman spectra on the four-layer sample described in the text. The calculated relative intensities of the folded lines (1 to 6) are given in the top of the figure, for a two-layer model (upper line) and a four-layer one (lower line). The asterisk labels a yet unidentified line.

to the $+n$ and $-n-1$ modes and the frequencies can be perfectly reproduced by the usual elastic model, assuming two layers in a period (60 Å for GaAs, 275 Å for AlAs). However the measured intensities of the lines do not display at all the usual trends. Similar observations have been recently published on some GaAs-AlAs three layers structures (8). These intensities can be however fully understood taking in account the correct geometry of the supercell. We give in Fig. 9 the calculated intensities, normalized to the one of line 1, for both simplified and real profile. The results are qualitatively different and the measured intensities only fit the four layers supercell predictions.

Let us now consider a usual GaAs-AlAs superlattice but with broaden interfaces. We previously published[15] Raman BS results on this type of samples and analyzed the frequencies of the confined optical modes and the intensities of the folded acoustical lines in terms of interface broadening. The average intensity of a given acoustic doublet was assumed to scale on the square of the corresponding Fourier component of the concentration profile. We then obtained a correct description of the decrease of this intensity as a function of interface broadening. With our more sophisticated model we recover similar results and we also predict a decrease of the doublet asymmetry with increasing interface broadening. This effect was not clearly seen previously and further experiments are currently in progress.

VII. CONCLUSION

In this paper we reviewed the theory of both the dispersion and light scattering activity of folded acoustical modes in superlattices. In a first approximation, the frequencies depend only on the superlattice period d, except at the zone center and zone edge where the gaps depend on the inner structure of the supercell. Forward Raman scattering experiments test the zone-center modes and allow to measure the corresponding gaps which, for a two abrupt monolayers superlattice, depend only on the average concentration x.

An easier experiment is to perform backward scattering which probes modes with finite wave vector Q. The relative intensities of a given acoustical doublet, contrary to the frequencies, drastically depend on the geometry of the supercell. They quantitatively reflect the softening of the zone-center photoelastic selection rules, which depends on Qd and on the zone-center gap magnitude. The analysis of both forward and backwards scattering experiments on a large set of GaAs-AlAs superlattices leads to an excellent quantitative agreement with the theoretical predictions.

Finally we would like to point out that a careful study of the intensities of the whole set of backscattering lines should allow the determination of the inner structure of the supercell of any sample.

ACKNOWLEDGMENTS

It is a pleasure for us to acknowledge J. Dubard for expert help in making the window selective etching and C. Colvard for an interesting discussion. Laboratoire de Bagneux is "Laboratoire Associé au Centre National de la Recherche Scientifique (LA 250)."

[1]For recent reviews see B. Jusserand and D. Paquet, in *Semiconductor Heterojunctions and Superlattices,* edited by N. Boccara, G. Allan, G. Bastard, M. Lannoo, and M. Voos (Springer, Berlin, 1986). See also M. V. Klein, in *Quantum Well Structures: Physics and Applications,* edited by D. S. Chemla and A. Pinczuk [IEEE J. Quantum Electron., special issue (1986)].

[2]S. M. Rytov, Akust. Zh. **2**, 71 (1956) [Sov. Phys.—Acoust. **2**, 68 (1956)].

[3]C. Colvard, R. Merlin, M. V. Klein, and A. C. Gossard, Phys. Rev. Lett. **45**, 298 (1980).

[4]J. Sapriel *et al.*, Phys. Rev. B **28**, 2007 (1983).

[5]B. Jusserand, D. Paquet, A. Regreny, and J. Kervarec, Solid State Commun. **48**, 499 (1983).

[6]C. Colvard *et al.*, Phys. Rev. B **31**, 2080 (1985).

[7]M. Nakayama *et al.*, Jpn. J. Appl. Phys. **24**, 1331 (1985).

[8]M. Nakayama, K. Kubota, S. Chika, H. Kato, and N. Sano, Solid State Commun. **58**, 475 (1986).

[9]B. Jusserand *et al.*, Appl. Phys. Lett. **46**, 678 (1985).

[10]S. Venugopalan, L. A. Kolodziejski, R. L. Gunshor, and A. K. Ramdas, Appl. Phys. Lett. **45**, 974 (1984).

[11]H. Brugger, G. Abstreiter, H. Jorke, H. J. Herzog, and E. Kasper, Phys. Rev. B **33**, 5928 (1986).

[12]J. Sapriel, J. C. Michel, J. C. Toledano, and R. Vacher, J. Phys. (Paris) Colloq. **45**, C5-139 (1984).

[13]B. Jusserand, F. Alexandre, J. Dubard, and D. Paquet, Phys. Rev. B **33**, 2897 (1986).

[14]M. Babiker, D. R. Tilley, and E. R. Albuquerque, J. Phys. C **18**, 1285 (1985).

[15]B. Jusserand, F. Alexandre, D. Paquet, and G. Le Roux, Appl. Phys. Lett. **47**, 301 (1985).

[16]G. Danan *et al.*, in the Proceedings of the 18th International Conference on Physics of Semicondoctors, Stockholm, 1986 (unpublished).

[17]S. Y. Ren and W. A. Harrison, Phys. Rev. B **23**, 762 (1981).

[18]S. Adachi and K. Oe, J. Appl. Phys. **54**, 6620 (1983).